CrossMark

Sol–gel synthesized BiFeO$_3$–Graphene nanocomposite as efficient electrode for supercapacitor application

S. Nayak[1] · Ankur Soam[2] · J. Nanda[1] · C. Mahender[2] · Mamraj Singh[3] · Debananda Mohapatra[4] · Rahul Kumar[5]

Abstract

In the present work, bismuth iron oxide–graphene composite has been explored as electrode material for electrochemical supercapacitor application. Bismuth iron oxide (BFO) nanoparticles, synthesized by sol–gel process, are mixed with the graphene sheets in a solution. The electrodes are prepared by coating the resulted slurry on stainless steel (SS) substrate, by drop casting process. The morphology and structure of the BFO–graphene composite are characterized by XRD, FIB-SEM, HRTEM and Raman spectroscopy, which show that the nanoparticles with diameter 100–200 nm are randomly distributed on and around the graphene sheets. The composite electrode exhibits significantly enhanced capacitance as compared to BFO. In this structure, the electrons generated by the surface based Faradaic reactions from the BFO nanoparticles can be transported by the graphene nanosheets toward the current collector. The electrochemical characteristic of the electrodes is investigated through cyclic voltammetry and charging/discharging process. The specific capacitance of the electrode measured at 5–100 mV/s was found to be 17–4 mF/cm^2 which is comparable to the most commonly used metal oxide based electrode materials. It shows better cycling stability with 95% retention of capacitance after 2000 cycles.

1 Introduction

Supercapacitors, the electrochemical energy storage devices, with high power density are considered as promising candidates in potential applications such as electric vehicles, wearable electronics, micro-electronic systems and industrial power and energy management [1–6]. In addition to higher power density, supercapacitor has larger cycle stability and faster charging/discharging rates over a battery, as it stores the charge at electrode's surface only. Supercapacitors are usually developed by selecting the electrode material, the electrolyte or the cell design to optimize the overall performance. Since the capacitance primarily depends on the electrode material, today's research is focused at exploring new electrode materials or modification in the existing electrode material to improve upon their capacitance [7–9]. Till date, many electrode materials have been studied for supercapacitor application. Supercapacitor electrodes are classified into two main categories based on the charge storage mechanisms; (1) metal oxides for pseudocapacitor [10, 11] and (2) carbon and silicon based materials for electric double layer capacitor (EDLC) [12–14].

The primary charge storage mechanism in pseudocapacitors involves faradaic redox reactions that control the oxidation states of host materials, whereas the carbon and silicon generally store charge electrostatically at electrode and electrolyte interface in an EDL. The metal oxide electrodes exhibit higher energy density and storage capacity, but the slow storage and limited lifetime are their drawbacks. On the other hand, EDLCs exhibit high rate capability, but suffer with low energy density. Achieving larger energy density of a supercapacitor without losing their power density and rate capability is a challenging task.

The above issue can be addressed by combining the two charge storage mechanisms, which function simultaneously

✉ Ankur Soam
  ankursoam007@gmail.com

[1] Department of Physics, Siksha 'O' Anusandhan University, Khandagiri Square, Bhubaneswar, Odisha 751030, India

[2] Department of Mechanical Engineering, Siksha 'O' Anusandhan University, Khandagiri Square, Bhubaneswar, Odisha 751030, India

[3] Department of Physics, University of Rajasthan, Jaipur 302004, India

[4] Department of Chemical Science, Tata Institute of Fundamental Research (TIFR), Mumbai 400005, India

[5] National Centre for Photovoltaic Research and Education (NCPRE), Indian Institute of Technology Bombay, Mumbai 400076, India

depending on the nature of the electrode material [15–18]. It is inferred from literature that adding the carbonaceous materials such as carbon nanotubes and garphene, to the metal oxides improves the electrical conductivity and mechanical strength of the composite material. Graphene, the carbonaceous material is a right choice for electrode material for supercapacitor in an aqueous media. The high surface area, excellent conductivity, good capacitance value have made this material useful for supercapacitor applications. In this regard, Zhang et al. [18] have reported that the graphene–ZnO composite film based supercapacitor exhibited an enhanced capacitive behavior with better reversible charging/discharging ability and higher capacitance value in comparison to graphene electrode. In literature, graphene sheets have also been deposited on silicon nanowires to increase their areal capacitance [19].

Chemically deposited metal oxides thin films such as RuO_2, MnO_2, NiO, Fe_2O_3, SnO_2, perovskites have been used as electrodes in supercapacitor [10]. Chemical deposition methods are inexpensive and enable the synthesis of material at low temperature, thus avoiding the high temperature effect like interdiffusion, contamination etc. The perovskite, BFO is a well known multiferroic material at room temperature, which has a wide range of applications including memory storage, spintronics, sensors and photovoltaic [20–23]. Recent studies have also revealed that BFO, due to its band gap of ~ 2 eV and good chemical stability, can be used as a visible light responsive photo-catalytic material and an active material in photovoltaic devices [21]. Till date, very few reports are available on the BFO electrodes for supercapacitor application [24–26]. Lokhande et al. [25] have explored the pervoskite nanocrystalline porous BFO thin film for supercapacitor in an aqueous NaOH electrolyte, which showed the capacitance of 81 F/g. It exhibits multiple crystallite phases i.e. $BiFeO_3$, $Bi_2Fe_4O_9$, $Bi_3Fe_5O_{12}$, $Bi_4Fe_2O_9$ and $Bi_{46}Fe_2O_{72}$ [25]. The presence of these phases is beneficial for a supercapacitor as it has the capability for sustaining the changes in the phases during the charging and discharging process. The BFO nanoflake electrode has also been studied for supercapacitor with a specific capacitance of 72.2 F/g [26]. Sarkar et al. [24] have improved the capacitance of BFO by depositing it on TiO_2 nanotubes. Though this structure showed the specific capacitance in the range of 350–440 F/g, the fabrication of this electrode has multiple and complex steps i.e. growth of TiO_2 nanotubes at high temperature and followed deposition of BFO on them by electrophoretic deposition process.

We have investigated the use of BFO–graphene composite film as electrode material in electrochemical supercapacitor. The structural and microstructure characterizations of the film were performed through XRD, SEM, TEM and Raman spectrometer. The device was fabricated by sandwiching two identical electrodes separated by a separator.

The performance of supercapacitor based on BFO electrode with that of BFO–graphene electrodes have also been compared. The electrochemical properties ascertain the use of composite electrode in supercapacitor.

2 Experimental details

2.1 BFO nanoparticles synthesis

BFO nanoparticles were synthesized by sol–gel combustion method [21]. The chemical reagents used in this work were bismuth nitrate, iron nitrate, nitric acid and citric acid. First, bismuth nitrate was dissolved in 1 N nitric acid at 60 °C to form aqueous solution. 5 mM iron nitrate was added to the solution under constant magnetic stirring and heating. Citric acid was successively added to the resulting transparent solution in 2:1 molar ratio with metal ions with vigorous stirring for 2 h, which turns the solution into light brown. The solution was kept at 60 °C for several hours until a dried gel was obtained. The dried gel was placed in a hot air oven at 220 °C and allowed to be auto-ignited. Finally, the as-prepared dark brownish powder was ground and calcined at 500 °C for 3 h.

2.2 BFO–graphene nanocomposite film preparation and characterization

Figure 1 displays the systematic representation of the preparation steps of BFO–graphene nanocomposite films. First, the freshly prepared BFO nanoparticles were dispersed in DI water (30 ml) and polyvinyl alcohol (PVA) was also added to prohibit the agglomeration of BFO nanoparticles. The solution was heated at 60 °C under constant stirring. The graphene nanosheets with composition ratio of 1:10 to BFO were added to the solution and the stirring process was continued for 6 h. The concentration of BFO–graphene with water was maintained throughout by adding extra water intermediately. This precursor solution was used for the deposition of films (drop-casting) on two SS substrates of size 2 cm × 2 cm each. The films were finally annealed at a 250 °C for 1 h. The mass density of the BFO–graphene film was found to be 0.2 mg/cm². The crystal structure of the film was investigated by X-ray diffraction, (PANalytical X'pert PRO) with CuKα radiations. The surface morphology of the prepared film was observed by Focused ion beam scanning electron microscopes (FIB-SEM), Carl Zeiss Microscopy and TEM (Jeol, JEM 2100F). Further, Raman spectroscopy (Horiba, HR 8000, Argon laser 514.5 nm) was also employed to confirm the different phases of the composite film.
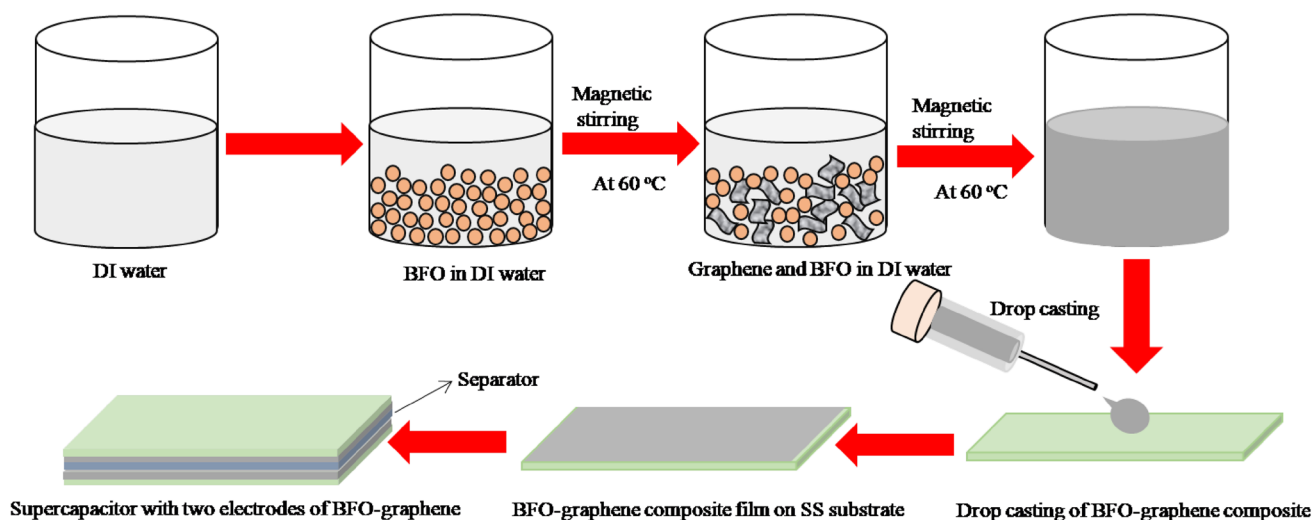
Fig. 1 Schematic representation of the processing steps for the fabrication of the electrodes of BFO–graphene composite and the supercapacitor

2.3 Device fabrication and electrochemical characterization

In this work, a supercapacitor was fabricated in two electrode configuration. The BFO–graphene composite film deposited on SS substrate acts as electrode. The device was assembled with a filter paper soaked in the electrolyte of 1 M Na_2SO_4 as a separator between the electrodes (shown in Fig. 1). For comparison, a device was also made with BFO film as electrodes. The electrochemical properties of the fabricated supercapacitor were analyzed through the Bio-Logic system (Model, SP-300) at room temperature. The capacitive properties were investigated from cyclic voltammetry (CV) and galvanostatic charging/discharging processes.

Fig. 2 XRD pattern of the BFO–graphene composite electrode

3 Results and discussion

The room temperature X-ray diffraction pattern of the BFO–graphene composite film is depicted in Fig. 2. The diffraction peaks are indexed to the distorted rhombohedral (R3c) structure of BFO (ICDD 01-086-1518). However, traces of small intensity phases are also observed. These two peaks are encircled and the magnified pattern is shown as inset to Fig. 2. The peak at 2θ of 27.7° indicates the presence of an impurity phase of $Bi_{25}FeO_{40}$ (ICDD 01-078-1543), whereas the presence of graphene sheets is confirmed by a graphite (multilayer graphene) peak at 2θ of 26.60°. This peak confirms interplanar stacking of the graphene sheets. Hence, the formation of BFO and graphene composite is confirmed by XRD analysis.

The morphology of the as-prepared BFO–graphene composite film is shown in the FIB-SEM image (Fig. 3). The graphene sheets exhibited flake type structure in BFO–graphene
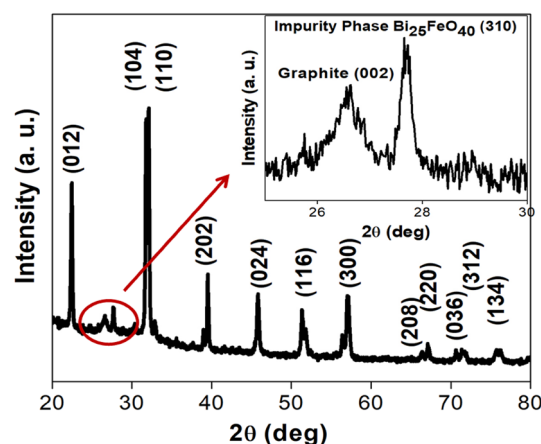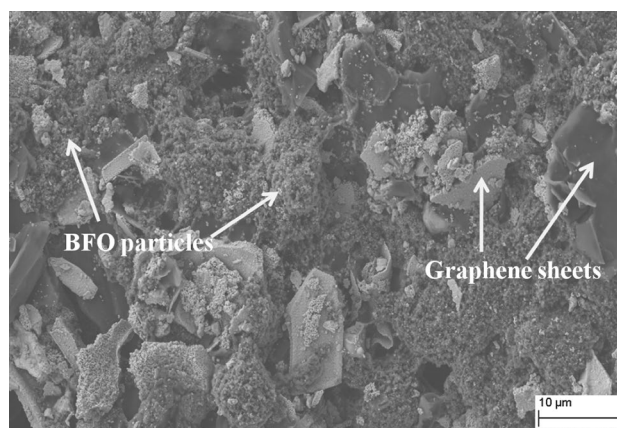

Fig. 3 FIB-SEM micrograph of the electrodes of BFO–graphene on SS substrate

film, with an average size of 5–10 μm. The BFO nanoparticles with size of 100–200 nm are observed to be randomly distributed around the graphene sheets as well as on the surface. The role of graphene is to increase the overall conductivity of the electrode and providing good transportation of charge between the electrode and the current collector. The graphene sheets are creating the separation/voids between the BFO particles, hence increasing the effective surface area of the composite film. This would definitely improve the capacitance of the supercapacitor.

HRTEM analysis (Fig. 4) was carried out in order to get the information of the morphology of the BFO particles and graphene sheets in the electrodes. For TEM, the material was removed from the electrode using acetone and then transferred on the Cu grid. Figure 4a shows the TEM image of the BFO–graphene composite. The coverage of graphene sheets with BFO particles can be observed from Fig. 4a. The BFO nanoparticles are present over the nanosheets (Fig. 4b) and this may prevent the aggregation of nanosheets

in the electrodes. The graphene exhibits rough texture as it has flexibility and ultrathin features. The composite of BFO–graphene has cavities within the electrode building a porous type structure for the electrode. The porous structure has better accessibility for the ions which is useful for the supercapacitor in high power application. Figure 4c shows the HRTEM image of the graphene sheets which have multilayered structure. The spacing between the graphene sheets is determined to be 0.329 nm which corresponds to the (002) plane. The TEM results are consistent with the XRD results shown earlier [27]. The energy dispersive X-ray spectroscopy (EDX) result of the composite electrode is shown in Fig. 4d.

Figure 5 shows the Raman spectrum of BFO–graphene film in the range of 100–2000 cm^{-1}. The spectrum exhibits two intense characteristic bands at 130 and 213 cm^{-1}, which correspond to A_1-1 and A_1-3 modes of BFO, respectively [28]. The presence $Bi_{25}FeO_{40}$ phase is confirmed by the band located at 518 cm^{-1} [29]. Two Raman bands are also
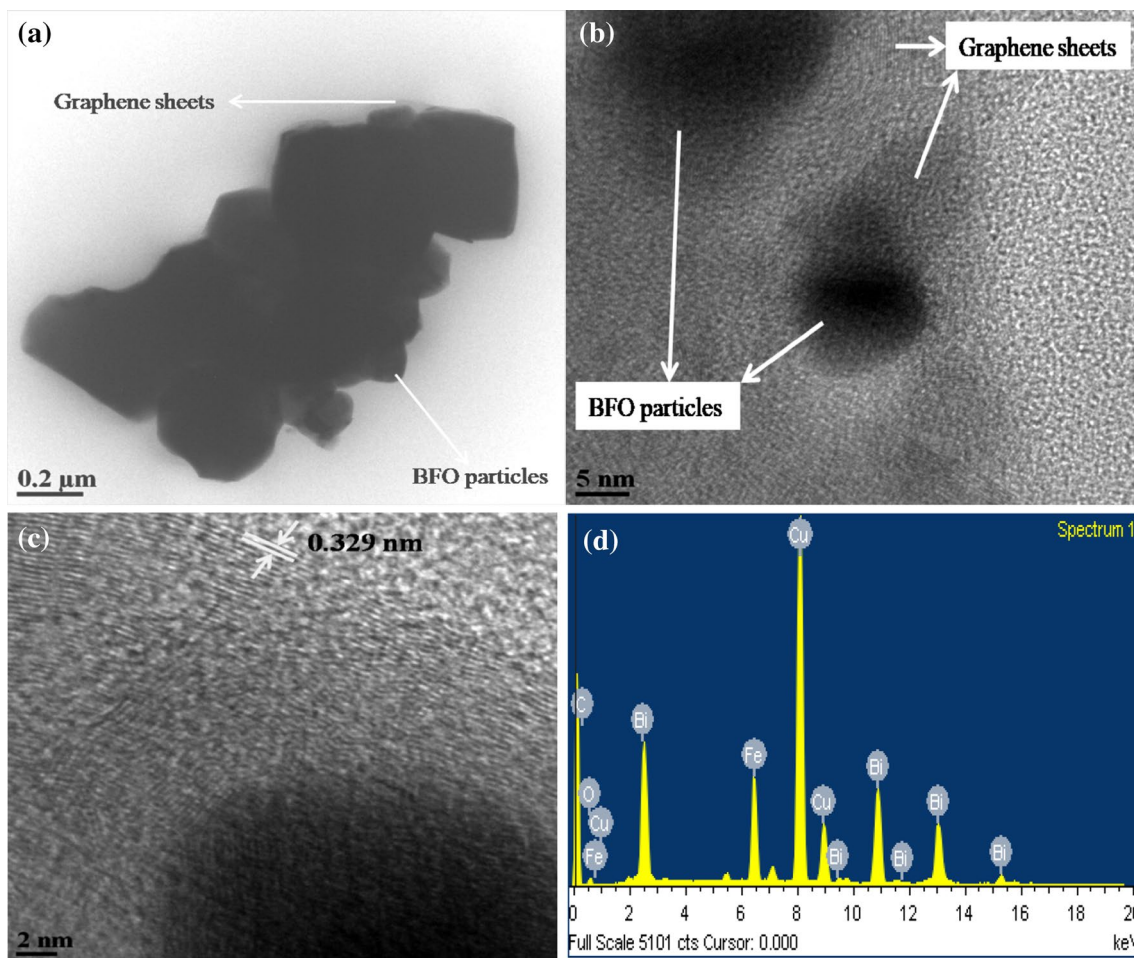

Fig. 4 **a** TEM photograph of the BFO–graphene composite, **b** magnified TEM image showing the BFO particles and graphene sheets, **c** HRTEM image of graphene sheets. The separation between graphene sheets is 0.329 nm which is corresponding to the interlayer distance. **d** EDX spectrum of the composite electrode
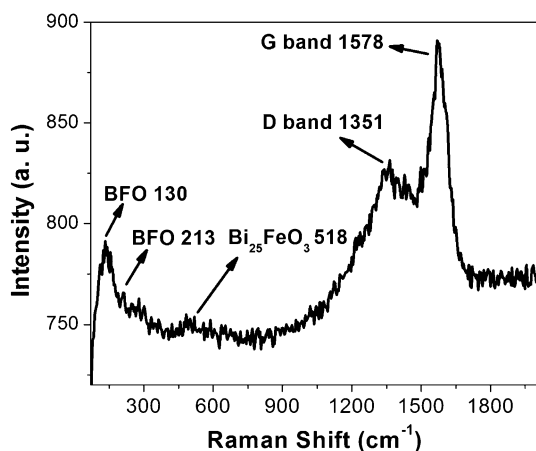
Fig. 5 Raman spectrum at room temperature of the BFO–graphene electrode

observed at ~ 1351 and ~ 1578 cm^{-1}, which are assigned to the carbonaceous materials (graphene sheets) [30]. G band (~ 1578 cm^{-1}) is a feature of the first order scattering of E_{2g} phonon of sp^2 bonded carbon atoms, and D band (~ 1351 cm^{-1}) is due to the breathing mode of K point phonons with A_{1g} symmetry, which generally occurs due the local defects and disorders in the graphene structure [19, 30].

To explore the BFO–graphene electrodes for supercapacitor application, the CV curves were recorded at scan rate of 20 mV/s. Figure 6a displays the difference between the CV curves of the constructed electrodes of BFO with and without graphene. The electrodes exhibit symmetric CV curves in forward and reverse sweep direction. The electrodes of BFO–graphene showed CVs with larger integrated area than BFO electrodes indicating enhancement in the capacitance. Moreover, the electrodes exhibit characteristics of an ideal supercapacitor (nearly rectangular shaped CV curves). This behavior is usually seen in case of carbon based electrodes [31]. In addition, a pair of redox reaction peaks is also observed in the CV curve.
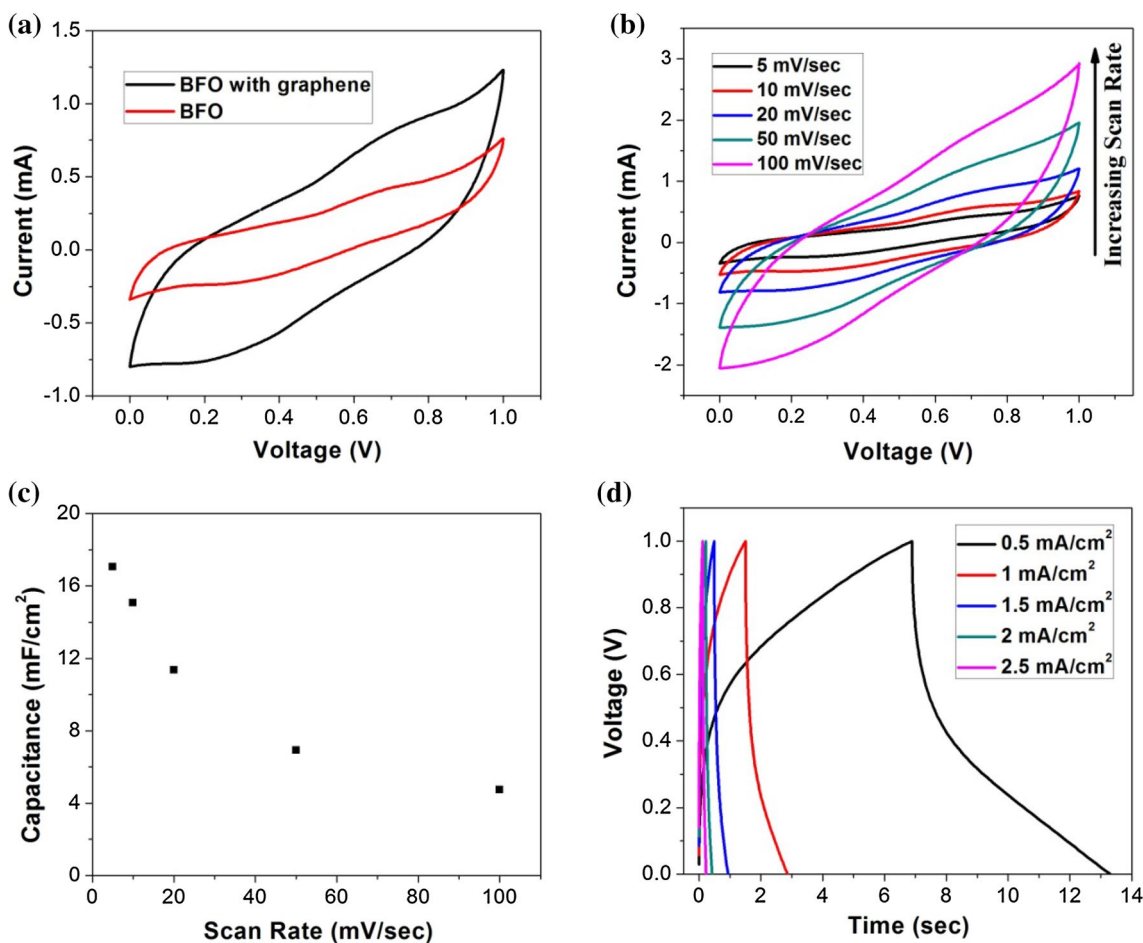

Fig. 6 **a** CV curves for electrodes deposited on SS substrate at a scan rate of 20 mV/s, **b** CV curves at different scanning rates for BFO–graphene composite electrodes, **c** effect of the scan rate on the electrode capacitance and **d** galvanostatic charging/discharging curves for BFO–graphene composite. The CV curves are recorded with 1 M Na_2SO_4 electrolyte

As seen from Fig. 6a, the capacitive current of BFO–graphene electrodes originates from the combination of two types of capacitances: (i) EDLC, where electrostatic storage is achieved by separating charges at the interface between the surface of the conductive electrode and an electrolyte, and (ii) pseudocapacitance, where faradaic electrochemical storage is achieved by redox reactions [25, 26]. Therefore, the composite electrodes exhibit higher capacitance output than BFO electrode. In literature, sarkar et al. [24] have also observed the redox peaks in CV from BFO. They have deposited a thin layer of BFO nanoparticles on TiO_2 nanotubes and the CV curves were evaluated in three electrode configuration [24]. Jadhav et al. [26] have reported the rectangular shaped CV curves for mixed-phase bismuth ferrite nanoflake with two electrode configuration.

From the CV curves (Fig. 6a), the areal capacitance of the electrodes was calculated using the equation

$$C \,(\text{areal capacitance}) = \frac{2 \times I}{S \times A}$$

where, I is the average current, A and S are the area of the electrode and the scan rate, respectively [7, 19]. BFO electrodes exhibit a capacitance of ~ 5.7 mF/cm^2, whereas by adding graphene sheets to the BFO electrodes it increases to ~ 11.35 mF/cm^2. This clearly indicates that the better capacitive properties for the BFO–graphene composite electrode. The capacitance per unit mass is determined to be 64 F/g at the scan rate of 20 mV/s. The specific capacitance values are observed to be comparable to the BFO based supercapacitors reported in the literature [25, 26]. However, this value is lower than the reported for the electrode of BFO coated on TiO_2 nanotube arrays [24]. Actually, the capacitance depends on various parameters such as the type of electrolyte and the measurement setup i.e. three electrode configurations or two electrode configurations. The specific capacitance of the BFO–graphene electrode is found to be higher than the bismuth oxide based electrodes with the same electrolyte (43 F/g at 5 mV/s) [32].

It has already been reported that the graphene with unique two-dimensional structure has good electrical conductivity and large surface area for supercapacitor as the both faces are available to accumulate the ions from the electrolyte forming two EDLs on a single sheet [18, 19, 33]. Moreover, graphene sheets would work as an excellent electron channel between the BFO nanoparticles and the substrate. The redox reactions from BFO contribute pseudocapacitance to the total capacitance of BFO–graphene electrode apart from the double-layer capacitance from graphene. Therefore, the higher electrical conductivity of the graphene and enhanced effective surface area of the electrode are the key points to improve the charge storage capacity of the electrode.

To study the effect of scan rates on the capacitance, the CV curves were further recorded at different scan rates

varying from 5 to 100 mV/s and shown in Fig. 6b. The current increases with the scan rate as expected usually. The rectangular shape of the CV curves of the composite electrode is less distorted with increase in voltage scan rates indicating its high charging/discharging rate capabilities. The maximum areal capacitance of 17 mF/cm^2 is obtained at the scan rate of 5 mV/s and it degrades to 4.75 mF/cm^2 at 100 mV/s (Fig. 6c). This electrode shows a better retention of capacitance at higher scan rates than the electrode of Mixed-phase bismuth ferrite nanoflake [26]. The capacitive behavior of the electrode also depends on the used electrolyte properties such as concentration, size of the ions, pH value. Therefore, a large number of electrolytes with different concentration have been used for supercapacitor application. BFO electrodes behavior has been tested with NaOH, KOH, Na_2SO_3, Na_2SO_4, NaCl and KCl electrolytes. Lokhande et al. [25] have achieved better performance from BFO in NaOH electrolyte. NaOH and KOH are corrosive and they may corrode the current collector which might cause the device failure or reduce cycle stability. In the present work, we have chosen the neutral electrolyte, Na_2SO_4. However, we have compared the electrochemical performance of the BFO based materials with different electrolytes reported in literature and presented in Table 1.

The decrease in the capacitance with the scan rate could be due to the following two mechanisms involved in the process: (1) the ions inaccessibility at the electrode surface at high charging/discharging rates due to slow diffusion rate of the ions and (2) the series resistance [35–37]. For BFO, the inner active sites may not follow the redox transitions completely at higher scan rates, resulting in decreasing the capacitance at such high scan rates. The full utilization of the electrode material can be achieved at slow scan rates. At higher scan rates BFO–graphene shows purely EDL capacitor behavior. The electrochemical performance was further investigate by recording charging/discharging curves within a voltage range of 0–1 V and varying the current densities from 0.5 to 2.5 mA/cm^2, as shown in Fig. 6d. It is clear that all curves while charging exhibit near linearity. However, during discharging there is an initial drop in the voltage caused by the inner resistances (IR drop), which can be reduced by finding an optimum ratio of BFO and graphene in the electrode.

The cycle life is an important parameter to evaluate the performance of any charge storage device. Thus the cycle life of the device was recorded by repeating the charging/discharging curves for 2000 cycles. Figure 7 displays the capacitance retention and coulombic efficiency as a function of cycle numbers. It can be seen that the composite electrode retained 95% of its initial capacitance after 2000 cycles, demonstrating its excellent electrochemical stability. Initially, it shows 98% coulombic efficiency and it decreases to 96% after 2000 cycles. BFO–graphene

Table 1 Comparison of the electrochemical performance of some selected bismuth metal oxide based electrodes

Electrode material	Electrolyte	Specific capacitance	Cycle stability	Ref.
Nanocrystalline porous bismuth iron oxide	1 M NaOH	81 F/g and 20 mF/cm^2 at 20 mV/s, 45 F/g and 11 mF/cm^2 at 200 mV/s (two electrode configuration)	Measured for 1000 cycles with slightly decrease in the capacitance	[25]
Mixed-phase bismuth ferrite nano-flake thin film	1 M NaOH	72.2 F/g at 1 A/g (three electrode configuration)	82.8% retention of the initial capacitance after 1500 cycles	[26]
Titania Nanotube/Bismuth Oxide Composite Electrode	1 M NaOH	185 mF/cm^2 at 20 mV/s (three electrode set up)	25% after 500 cycles	[34]
BiFeO$_3$ Anchored TiO$_2$ Nanotube Arrays	0.5 M Na$_2$SO$_4$	440 F/g at 1.1 A/g 350 F/g at 2.5 A/g (three electrode configuration)	92.5 retention after 1200 cycles	[24]
γ-Bi$_2$MoO$_6$ nanoplates	1 M Na$_2$SO$_4$ 1 M NaOH	43 F/g in 1 M Na$_2$SO$_4$, and 519 F/g in 1 M NaOH (three electrodes cell)	About 80% retention after 30 cycle after that stable upto 200 cycle	[32]
BiFeO$_3$–Graphene nanocomposites	1 M Na$_2$SO$_4$	17−4 mF/cm^2, at 5–100 mV/s 64 F/g at the scan rate of 20 mV/s (two electrode setup)	95% retention after 2000 cycles	Pres-ent work
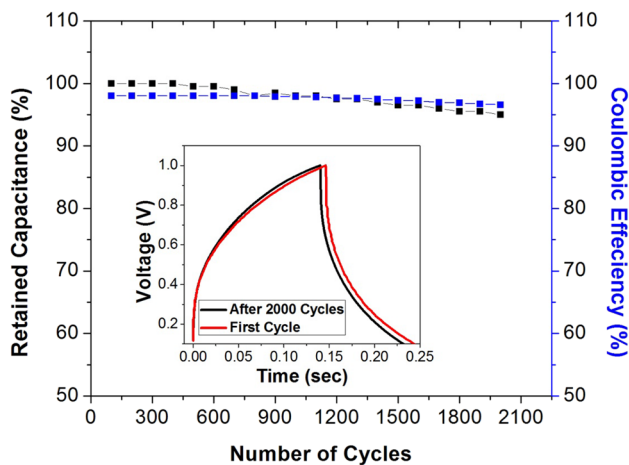
Fig. 7 Cycle stability of the supercapacitor fabricated with BFO–graphene composite electrodes

electrode exhibits better capacitance retention than BFO/TiO$_2$ [24] and pure mixed-phase bismuth ferrite [26] electrodes. These results indicate that the BFO–graphene electrode can be used for high performance supercapacitor with long term stability. The better performance of the BFO–graphene composite electrode can be attributed to the synergistic effects of the electrochemical properties of graphene sheets and BFO particles. BFO nanoparticles prevent the restacking and agglomeration of graphene sheets. Thus BFO nanoparticles act as an agent for the building a 3D interconnected conductive porous structure to improve the electrical conductivity and fast charge transport within the electrode. Graphene sheets are compatible to oxide function group, which increases the available surface area, thus enhancing the total capacitance of the electrode.

4 Conclusions

In summary, a composite electrode of BFO–graphene has been developed and tested for supercapacitor application in an aqueous electrolyte of 1 M Na$_2$SO$_4$. The capacitance of the BFO with graphene has been observed to be significantly larger than that of without graphene. The increase in the capacitance is mainly attributed to the enhancement of the electrical conductivity and the surface area of the electrode after adding graphene sheets. The device exhibited a good electrochemical stability with a loss of capacitance of 5% with coulombic efficiency of ~96% after 2000 cycles. Optimization for the concentration of BFO and graphene can further improve the device performance. Therefore, this work suggests that this hybrid electrode of metal oxides with carbon based materials has promising potential in the application of energy storage devices.

References

1. R. Kotz, M. Carlen, Principles and applications of electrochemical capacitors. Electrochim. Acta **45**, 2483–2498 (2000)

2. S.F. Tie, C. Wei, A review of energy sources and energy management system in electric vehicles. Renew. Sustain. Energy Rev. **20**, 82–102 (2013)

3. A. Kuperman, I. Aharon, Battery—ultracapacitor hybrids for pulsed current loads: a review. Renew. Sustain. Energy Rev. **15**, 981–992 (2011)

4. J.R. Miller, A.F. Burke, Electrochemical capacitors: challenges and opportunities for real-world applications. Electrochem. Soc. Interface **17**, 53–57 (2008)

5. D.P. Dubal, G. Kim, Y. Kim, R. Holze, C.D. Lokhande, W.B. Kim, Supercapacitors based on flexible substrates: an overview. Energy Technol. **2**, 325–341 (2014)

6. T. Lé, P. Gentile, G. Bidan, D. Aradilla, New electrolyte mixture of propylene carbonate and butyltrimethylammonium bis(trifluoromethylsulfonyl)imide (N1114 TFSI) for high performance silicon nanowire (SiNW)-based supercapacitor applications. Electrochim. Acta **254**, 368–374 (2017)

7. M.K. Hota, Q. Jiang, Y. Mashraei, K.N. Salama, H.N. Alshareef, Fractal electrochemical microsupercapacitors. Adv. Electron. Mater. **3**, 1700185 (2017)

8. K. Zhang, L.L. Zhang, X.S. Zhao, J. Wu, Graphene/polyaniline nanofiber composites as supercapacitor electrodes. Chem. Mater. **22**, 1392–1401 (2010)

9. L. Gurusamy, S. Anandan, J.J. Wu, Synthesis of reduced graphene oxide supported flower-like bismuth subcarbonates microsphere ($Bi_2O_2CO_3$-RGO) for supercapacitor. Appl. Electrochim. Acta **244**, 209–221 (2017)

10. C.D. Lokhande, D.P. Dubal, O. Joo, Metal oxide thin film based supercapacitors. Curr. Appl. Phys. **11**, 255–270 (2017)

11. Q.J. Le, T. Wang, D.N.H. Tran, F. Dong, Y.X. Zhang, D. Losic, Morphology-controlled MnO_2 modified silicon diatoms for high-performance asymmetric supercapacitors. J. Mater. Chem. A **5**, 10856–10865 (2017)

12. A. Soam, N. Arya, A. Singh, R. Dusane, Fabrication of silicon nanowires based on-chip micro-supercapacitor. Chem. Phys. Lett. **678**, 45–50 (2017)

13. E. Frackowiak, K. Metenier, V. Bertagna, F. Beguin, Supercapacitor electrodes from multiwalled carbon nanotubes. Appl. Phys. Lett. **77**, 2421–2423 (2010)

14. A.G. Pandolfo, A.F. Hollenkamp, Carbon properties and their role in supercapacitors. J. Power Sources **157**, 11–27 (2006)

15. P. Chen, G. Shen, S. Sukcharoenchoke, C. Zhou, Flexible and transparent supercapacitor based on In $_2O_3$ nanowire/carbon nanotube heterogeneous films. Appl. Phys. Lett. **94**, 043113 (2009)

16. A.L.M. Reddy, S. Ramaprabhu, Nanocrystalline metal oxides dispersed multiwalled carbon nanotubes as supercapacitor electrodes. J. Phys. Chem. C **111**, 7727–*7734* (2007)

17. V. Khomenko, E. Frackowiak, F. Be, Performance of manganese oxide CNTs composites as electrode materials for electrochemical capacitors. J. Electrochem. Soc. **152**, 229–235 (2005)

18. Y. Zhang, H. Li, L. Pan, T. Lu, Z. Sun, Capacitive behavior of graphene—ZnO composite film for supercapacitors. J. Electroanal. Chem. **634**, 68–71 (2009)

19. A. Soam, P. Kavle, A. Kumbhar, R.O. Dusane, Performance enhancement of micro-supercapacitor by coating of graphene on silicon nanowires at room temperature. Curr. Appl. Phys. **17**, 68–71 (2017)

20. H. Wu, J. Zhou, L. Liang, L. Li, X. Zhu, Fabrication, characterization, properties, and applications of low-dimensional $BiFeO_3$ nanostructures. J. Nanomater. **2014**, 471485 (2014)

21. S. Nayak, C. Mahender, S. Ankur, J. Nanda, Structural and optical studies of $BiFeO_3@SiO_2$ core/shell nanoparticles. Mater. Res. Express **4**, 105029 (2017)

22. L. Di, H. Yang, T. Xian, X. Chen, Enhanced photocatalytic activity of $NaBH_4$ reduced $BiFeO_3$ nanoparticles for rhodamine B decolorization. Materials **10**, 1118 (2017)

23. P. Banerjee, A.F. Jr, Influence of Y and Co co-doping in the multiferroic behaviors of $BiFeO_3$ ceramics. J. Mater. Sci. **28**, 8562–8568 (2017)

24. A. Sarkar, A.K. Singh, D. Sarkar, G.G. Khan, K. Mandal, Three-dimensional nanoarchitecture of $BiFeO_3$ anchored TiO_2 nanotube arrays for electrochemical energy storage and solar energy conversion. ACS Sustain. Chem. Eng. **3**, 2254–2263 (2015)

25. C. Lokhande, T. Gujar, R.S. Mane, S.H. Han, Electrochemical supercapacitor application of pervoskite thin films. Electrochem. Commun. **9**, 1805–1809 (2007)

26. V.V. Jadhav, M.K. Zate, S. Liu, M. Naushad, R.S. Mane, K.N. Hui, S.H. Han, Mixed-phase bismuth ferrite nanoflake electrodes for supercapacitor application. Appl. Nanosci. **6**, 511–519 (2016)

27. M.P. Tereza, A.K. Thapa, A. Sherehiy, J.B. Jasinski, J.S. Jangam, Incommensurate graphene foam as a high capacity lithium intercalation anode. Sci. Rep. **7**, 39944 (2017)

28. P. Priyadharsini, A. Pradeep, B. Sathyamoorthy, G. Chandrasekaran, Enhanced multiferroic properties in La and Ce. J. Phys. Chem. Solids **75**, 797–802 (2014)

29. A. Sun, H. Chen, C. Song, F. Jiang, X. Wang, Y. Fu, Magnetic $Bi_{25}FeO_{40}$-graphene catalyst and its high visible-light photocatalytic performance. RSC Adv. **3**, 4332–4340 (2013)

30. A. Kaniyoor, S. Ramaprabhu, A Raman spectroscopic investigation of graphite oxide derived graphene. AIP Adv. **2**, 032183 (2012)

31. H. Pan, J. Li, Y.P. Feng, Carbon nanotubes for supercapacitor. Nanoscale Res. Lett. **5**(3), 654–668 (2010)

32. B. Senthilkumar, R.K. Selvan, L. Vasylechko, M. Minakshi, Synthesis, crystal structure and pseudocapacitor electrode properties of γ-Bi_2MoO_6 nanoplates. Solid State Sci. **35**, 18–27 (2014)

33. W. Liu, C. Lu, X. Wang, R.Y. Tay, B.K. Tay, High-performance microsupercapacitors based on two-dimensional graphene/manganese dioxide/silver nanowire ternary hybrid film. ACS Nano **9**, 1528–1542 (2015)

34. B. Sarma, A.L. Jurovitzki, Y.R. Smith, S.K. Mohanty, M. Misra, Redox-induced enhancement in interfacial capacitance of the titania nanotube/bismuth oxide composite electrode. ACS Appl. Mater. Interface*s* **5**, 1688–1697 (2013)

35. W.G. Pell, B.E. Conway, Analysis of power limitations at porous supercapacitor electrodes under cyclic voltammetry modulation and dc charge. J. Power Sources **96**, 57–67 (2001)

36. W.G. Pell, B.E. Conway, N. Marincic, Analysis of non-uniform charge/discharge and rate effects in porous carbon capacitors containing sub-optimal electrolyte concentrations. J. Electroanal. Chem. **491**, 9–21 (2000)

37. R.D. Levie, On porous electrodes in electrolyte solutions: I. capacitance effects. Electrochim. Acta **8**, 751–780 (1963)